ISSN (Print) 1226-1750
ISSN (Online) 2233-6656
Journal of Magnetics 23(3), 375-380 (2018) https://doi.org/10.4283/JMAG.2018.23.3.375

Attenuation Effect of PET Images with and Without the Magnetic Resonance Breast Coil using Various MR Attenuation Correction Sequences

Chan Rok Park[1,2], Youngjin Lee[3], and Hyungjin Yang[1]*

[1]*Department of Biomedical Science, Korea University, 2511, Sejong-Ro, Sejong-City 30019, Republic of Korea*
[2]*Department of Nuclear Medicine, Seoul National University Hospital, 101, Daehak-Ro, Jongno-Gu, Seoul 03080, Republic of Korea*
[3]*Department of Radiological Science, Gachon University, 191, Hambakmoe-Ro, Yoensu-Gu, Incheon 21936, Republic of Korea*

(Received 18 July 2018, Received in final form 19 September 2018, Accepted 20 September 2018)

The present study aims to confirm the attenuation correction (AC) in positron emission tomography (PET) images using various magnetic resonance (MR) sequences with and without the MR breast radiofrequency (RF) coil, and thus to evaluate the attenuation effect of the MR breast RF coil. To that purpose, we reconstructed non-attenuated PET data using the MR $AC_{Dixon\text{-}CAIPI}$, MR AC_{UTE}, and MR $AC_{Dixon\text{-}GRAPPA}$ sequences. The results indicated that the signal loss of the PET image with the MR breast RF coil was the lowest when the MR $AC_{Dixon\text{-}GRAPPA}$ sequence was applied. In conclusion, the MR $AC_{Dixon\text{-}GRAPPA}$ sequence maintained PET image quality when using the MR breast RF coil during PET/MR scanning.

Keywords : PET/MR, MR-based attenuation correction sequences, Breast PET/MR RF coil

1. Introduction

The combined positron emission tomography (PET) and magnetic resonance (MR) technique, known as simultaneous PET/MR, provides functional and molecular information through PET, as well as superior soft tissue information and uses an attenuation correction map derived from the MR data to correct the PET image [1]. PET/MR is associated with lower radiation exposure than PET/CT. Various MR sequences and contrast agents aid clinicians in ascertaining disease stage [2-4].

Conventional MR breast imaging uses the dedicated MR breast radiofrequency (RF) coil to receive and transmit MR signals [5, 6]. In PET/MR scanning, the dedicated MR breast RF coil, which contains attenuation and scatter materials, is positioned between the patient and the PET detector and may therefore decrease PET signal loss due to MR hardware [7]. Many researchers have reported that MR hardware reduced PET count in PET/MR [8-11]. Delso *et al.* reported a ~17 % decrease in PET quality when using the MR RF coil [8], Isabel *et al.* estimated that the MR breast RF coil led to a 22 % underestimation in the PET standard uptake value (SUV) during PET/MR scanning [9]. In PET/CT, to acquire a good quality of PET image, attenuation correction is performed by converting the CT-acquired Hounsfield units (HU) using a 511-keV attenuation coefficient, because a similar physical interaction occurs between an X-ray and a 511-keV photon [12]. In PET/MR, attenuation correction is performed by acquiring either the ultrashort echo time (UTE) sequence or the T1-weighted two-point Dixon 3D volumetric interpolated breath-hold examination sequence [13]. The Dixon sequence uses two echo times to create a fat and water image that is acquired in and out of phase.

Soft tissues can be divided into four categories: background, lungs, fat, and soft tissue by using the Dixon sequence [14]. In PET/MR, attenuation coefficients are assigned to these different types of tissues to generate an MR-based attenuation map for the PET image. The generalized autocalibrating partially parallel acquisition (GRAPPA) algorithm ensures higher sensitivity and good spatial resolution in MR-based attenuation correction (MR AC; MR $AC_{Dixon\text{-}GRAPPA}$). This algorithm accelerates the acquisition of MR data by imaging the under-sampled k-space and then compensating for the k-space values by approximating the MR data that are missed during the short acquisition time [15]. In addition, controlled aliasing in parallel imaging results in higher acceleration (CAIPIRINHA) algorithm is an expanded GRAPPA algorithm (MR $AC_{Dixon\text{-}CAIPI}$) [16, 17]. It requires a shorter

*Corresponding author: Tel: +82-44-860-1325
Fax: +82-44-860-1325, e-mail: yangh@korea.ac.kr

acquisition time (9 sec) and therefore usually improves the high-resolution MR images, because the images should be acquired during one breath-hold time and as such, a long acquisition interval is not feasible. In addition, the UTE MR sequence acquires highly reduced two-echo time images (MR AC_{UTE}) [18]. In this regard, Keereman *et al.* demonstrated that the UTE sequence was more effective for cortical bone attenuation correction [19]. In summary, it is clear that the attenuation of the PET image is corrected using various MR sequences and algorithms.

The aim of the present study was to investigate the attenuation effect in MR-based PET images with and without MR breast RF coils. The quality of the MR AC PET phantom images was evaluated using three MR attenuation correction sequences (MR $AC_{Dixon\text{-}CAIPI}$, MR AC_{UTE}, and MR $AC_{Dixon\text{-}GRAPPA}$).

2. Materials and Methods

2.1. Simultaneous PET/MR

An integrated PET/MR scanner was used in all examinations (Biograph mMR; Siemens, Germany). This 3.0-T PET/MR equips an excellent gradient system that generates a maximum amplitude of 45 mT/m and a maximum slew rate of 200 T/m/s. The PET detector consists of 8 × 8 lutetium oxyorthosilicate (LSO) scintillator crystals, 8 detector rings, 56 detector blocks, and a 3 × 3 avalanche photodiode array; it is located between the MR gradient coil and the MR breast RF coil. The PET detector covers a field of view (FOV) of 59.4 cm in the transverse direction and 25.8 cm in the axial direction. To carry out the breast PET/MR scan, an MR breast RF coil (MR-BI320-PA; Noras MRI Products GmbH, Germany) was used on the scanner table.

2.2. PET acquisition

As shown in Fig. 1(a), the MR breast RF coil was positioned at the center of the table to evaluate the attenuation effect. Figure 1(b) shows the cylindrical phantom without the MR breast RF coil. When we simulated the

(a) (b)

Fig. 1. (Color online) Breast PET/MR phantom image (a) with and (b) without the MR breast RF coil.

Table 1. Acquisition parameters.

MR parameters	MR $AC_{Dixon\text{-}CAIPI}$	MR AC_{UTE}	MR $AC_{Dixon\text{-}GRAPPA}$
Acquisition time	00:08	01:58	00:19
Voxel size (mm)	2.6 × 2.6 × 3.1	1.6 × 1.6 × 1.6	2.6 × 2.6 × 3.1
Matrix size	264 × 352	192 × 192	192 × 126
Field of view (mm)	500	300	500
Repetition time (ms)	4.26	11.94	3.60
Echo time (ms)	1.24 / 2.47	0.07 / 2.46	1.23 / 2.46
PET Reconstruction			
Acquisition time	10 min		
Reconstruction		3D OSEM (Iterations : 3, Subsets : 21)	
Post filter		Gaussian filter (6 mm)	
Matrix size		172 × 172	

AC: Attenuation correction, CAIPIRINHA: Controlled aliasing in parallel imaging results in higher acceleration, GRAPPA: generalized autocalibrating partially parallel acquisition, UTE: Ultra short echo time.

phantom test, we used styrofoam to fix the cylindrical phantoms, which were designed to mimic the shape of the breast. The cylindrical phantoms were filled with an ^{18}F solution with 37 kBq/mL of radioactivity. All PET data were acquired for 10 minutes and then reconstructed using MR $AC_{Dixon\text{-}CAIPI}$, MR AC_{UTE}, and MR $AC_{Dixon\text{-}GRAPPA}$. Table 1 indicates the acquisition parameters.

2.3. Data analysis

For the analysis, we used Amide's a Medical Image Data Examiner (AMIDE) software. Figure 2 shows the attenuation corrected PET image drawn as an ROI with an inner diameter of 2 cm. With and without the MR breast RF coil, we measured the average count and standard deviation at the center of the slices. To evaluate the attenuation effect of the PET image with and without the MR breast RF coil, SNR and percentage NU were calculated.

$$\mathrm{SNR} = \frac{\text{Average Count of Activity } (C_k)}{\text{Standard Devication of Counts } (C_k)},$$

where the subscript *k* of C indicates an ROI with an inner diameter of 2 cm in the center slice of the PET image. The Average Count of Activity (C_k) is the average count of an ROI in the center slice of a PET image. Standard Deviation of Counts (C_k) is the standard deviation of the counts within an ROI in the center slice of a PET image.

The NU (%) is calculated as follows:

$$\mathrm{NU}(\%) = \frac{\mathrm{Max}(C_k) - \mathrm{Ave}(C_k)}{\mathrm{Ave}(C_k)} \times 100,$$

where the subscript *k* of C refers to an ROI with an inner diameter of 2 cm in the center slice of a PET image. Max (C_k) is the maximum count within an ROI in the center slice of a PET image, and Ave (C_k) is the average count within an ROI in the center slice of a PET image.

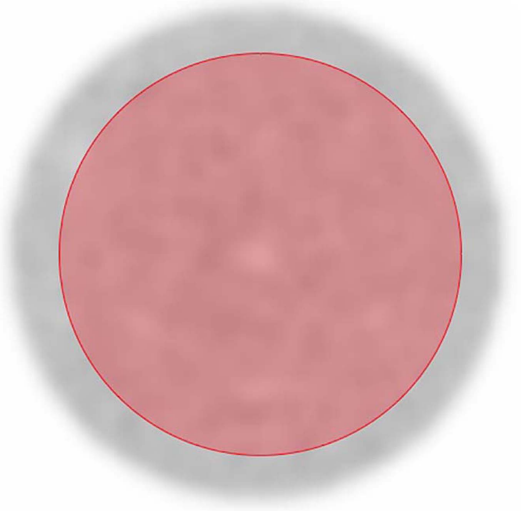

Fig. 2. (Color online) MR-based attenuation correction PET image drawn as a region of interest (diameter: 2 cm).

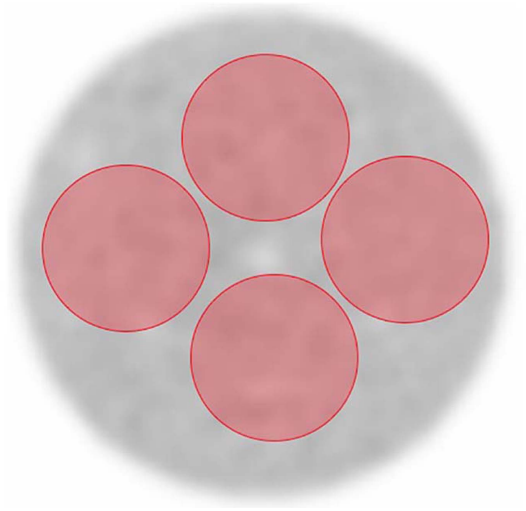

Fig. 3. (Color online) MR-based attenuation correction PET image drawn as a region of interest (diameter: 1 cm) according to position (upper, bottom, right, and left).

In addition, attenuation effect was investigated in 10 slices of an ROI with an inner diameter of 2 cm. And PET images applying for MR $AC_{Dixon\text{-}CAIPI}$, MR AC_{UTE}, and MR $AC_{Dixon\text{-}GRAPPA}$ were evaluated by using average counts. Figure 3 shows an attenuation-corrected PET image drawn as an ROI with an inner diameter of 1 cm, according to position (upper, bottom, right and left) at the center of the slices. This PET image was analyzed with and without the MR breast RF coil to confirm attenuation effect of position.

3. Results and Discussion

Table 2 shows the degree of attenuation of the PET images with and without the MR breast RF coil. In comparison with the PET images applied to the three MR AC sequences, the PET image with the MR breast RF coil had a SNR that was decreased by 15.0 %, a standard deviation that was increased by 16.9 %, and a percentage NU that was increased by 26.4 %. Figure 4 shows the percentage NU of the PET images applied to the three MR AC sequences. The MR AC_{UTE} PET image showed no difference in NU with or without the MR breast RF coil. However, the percentage NU of the MR AC_{UTE} PET images was the highest among the PET images applied to the three MR AC sequences. In a comparison between the MR $AC_{Dixon\text{-}CAIPI}$ and MR $AC_{Dixon\text{-}GRAPPA}$ PET images, the

Table 2. Average count, standard deviation, and signal-to-noise ratio in the three MR-based attenuation correction sequences.

	MR $AC_{Dixon-CAIPI}$				MR AC_{UTE}				MR $AC_{Dixon-GRAPPA}$			
	AC	SD	SNR	NU	AC	SD	SNR	NU	AC	SD	SNR	NU
W-coil	49525.0	4223.0	11.7	19.6	72485.0	7800.0	9.3	24.7	50473.0	4829.0	10.5	22.9
W/O coil	65158.0	3831.0	17.0	11.3	83425.0	6115.0	13.6	23.2	54421.0	4468.0	12.2	12.3

AC: Average count, SD: Standard deviation, SNR: Signal to noise ratio, NU: Non-uniformity (%).

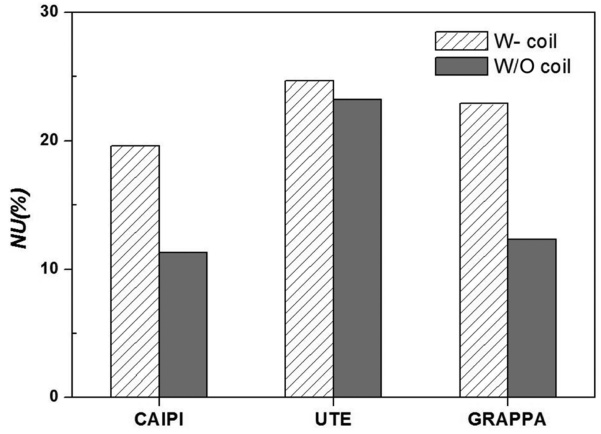

Fig. 4. Percentage difference in non-uniformity between the MR $AC_{Dixon-CAIPI}$, MR AC_{UTE}, and MR $AC_{Dixon-GRAPPA}$ PET images.

NU of the PET image taken with the MR breast RF coil was 1.7 and 1.8 times higher than the PET image taken without the coil, respectively. Similarly, compared with all MR AC PET images, the percentage NU was 22.4 % in the MR breast RF coil and 15.6 % in the images without the MR breast RF coil. The percentage NU of the PET image with the MR breast RF coil was higher than that of the PET image without the MR breast RF coil.

Figure 5 compares the average count of the PET images taken using the various MR AC sequences in the 10 slices with and without the MR breast RF coil. In the PET images subjected to MR $AC_{Dixon-CAIPI}$, MR AC_{UTE} and MR $AC_{Dixon-GRAPPA}$, the average-count was decreased by 25.2 %, 14.5 %, and 6.5 %, respectively.

Figures 6 and 7 show the percentage difference in average-count position with and without the MR breast RF coil. According to position (upper, bottom, right, and left), the percentage differences were 22.9 %, 25.0 %, 26.0 %, and 25.1 % in the MR $AC_{Dixon-CAIPI}$ PET images, 12.2 %, 17.7 %, 14.7 %, and 7.1 % in the MR AC_{UTE} PET images, and 9.8 %, 9.6 %, 2.2 %, and 5.4 % in the MR $AC_{Dixon-GRAPPA}$ PET images.

Thus, we were able to confirm the difference of the attenuation effect of PET images using three MR AC sequences with and without the MR breast RF coil. In a comparison of the three MR AC PET sequences, the

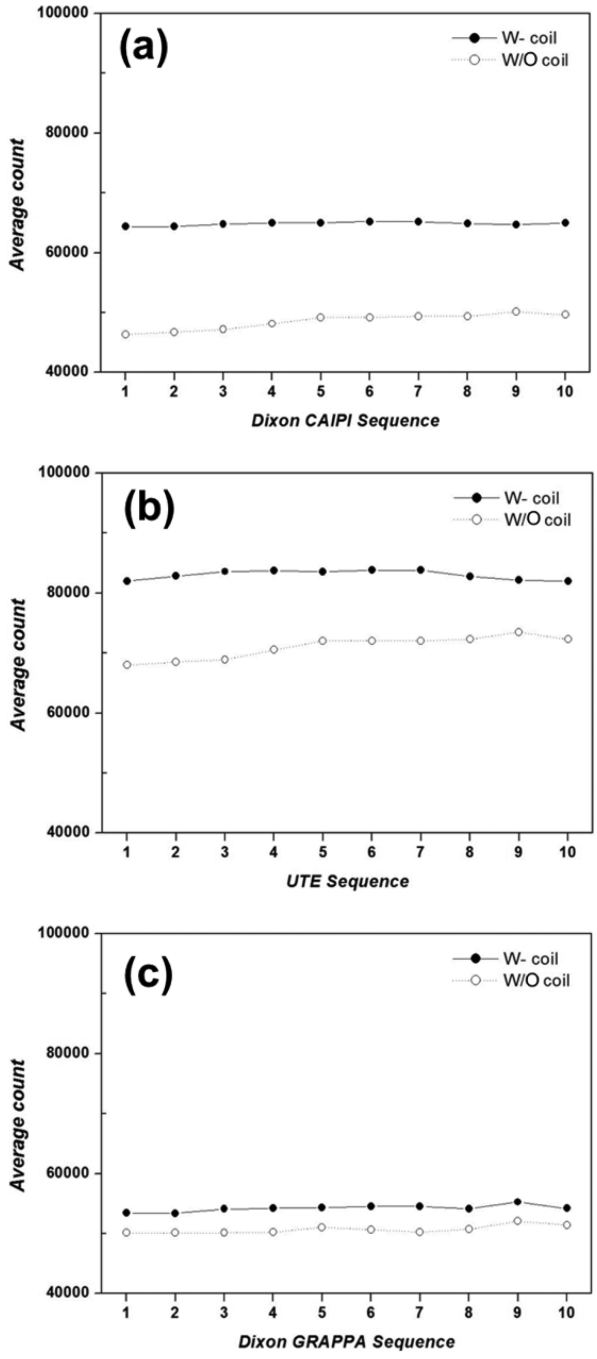

Fig. 5. Average count of PET images using (a) MR $AC_{Dixon-CAIPI}$, (b) MR AC_{UTE}, and (c) MR $AC_{Dixon-GRAPPA}$ in 10 slices with and without the MR breast RF coil.

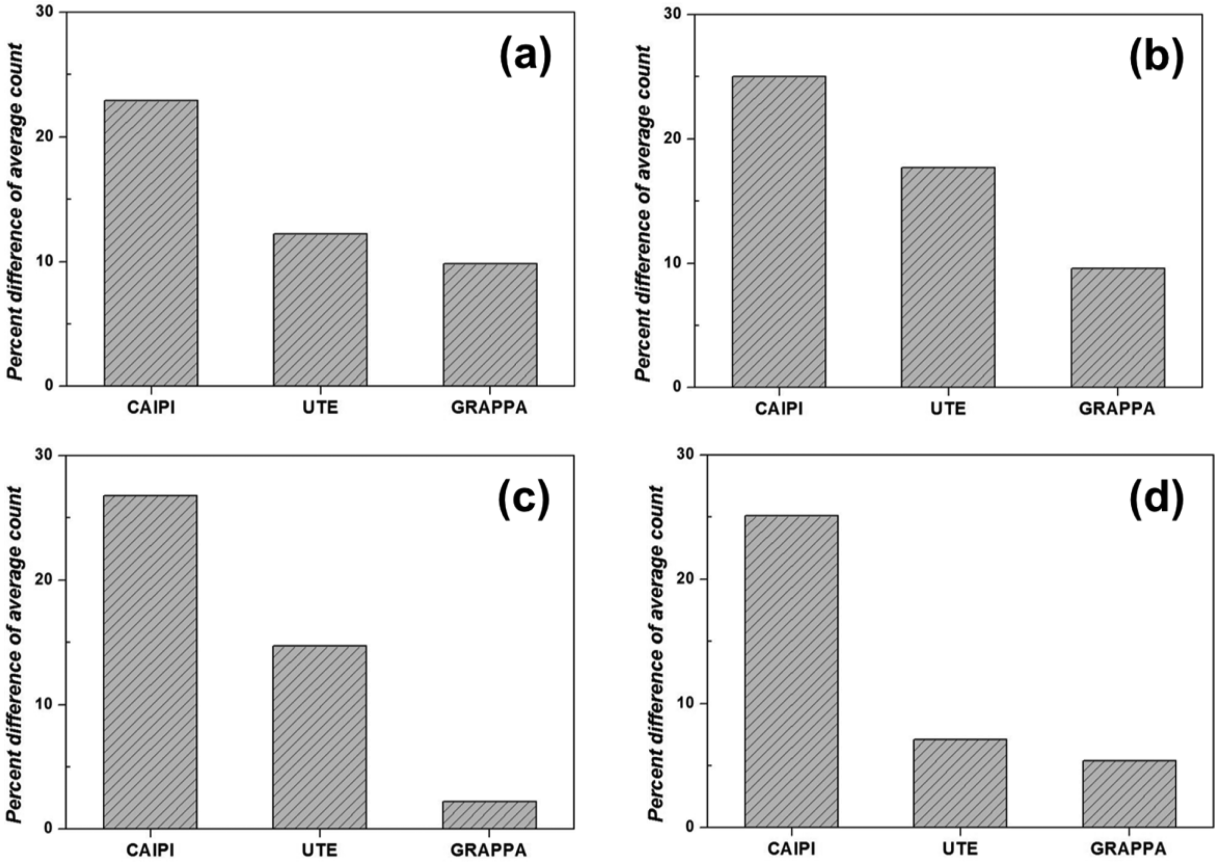

Fig. 6. Percentage difference in average count with and without the MR breast RF coil, according to position, as follows: (a) upper, (b) bottom, (c) right, and (d) left.

acquisition time was shortest in the MR $AC_{Dixon\text{-}CAIPI}$ PET images, although the highest PET average count loss using the MR breast RF coil also occurred in those images. The MR AC_{UTE} PET image, required a long acquisition time—about 2 minutes. This limits its usefulness to patients, who need to hold their breath for the whole-body PET/MR scan. Nonetheless, many researchers have reported that the MR AC_{UTE} sequence is effective for brain PET/MR [20, 21]. Average-count acquisition was also highest in the MR AC_{UTE} sequence among the three MR AC PET images. However, the SNR was low because there was a high standard deviation. The MR $AC_{Dixon\text{-}GRAPPA}$ PET image indicated that this sequence had less effect on the difference rate of PET average count with and without the MR breast RF coil.

4. Conclusion

In the present study, we compared and analyzed PET image quality with and without the MR breast RF coil using three different MR AC sequences. The quality of PET images was evaluated in terms of SNR, NU, and average count. Unlikely the previous study, we were able to evaluate PET images based on various MR AC sequences with and without MR breast RF coil. We confirmed that the MR breast RF coil decreased PET image quality, for the average count within the ROI, the standard deviation and the uniformity of the average count, and the SNR for all the MR AC sequences. In a comparison among the MR $AC_{Dixon\text{-}CAIPI}$, MR AC_{UTE}, and MR $AC_{Dixon\text{-}GRAPPA}$ PET images, the MR $AC_{Dixon\text{-}GRAPPA}$ PET images exhibited smaller differences for the SNR, NU, and average-count with and without the MR breast RF coil, compared to the other images, as shown in Table 2 and Fig. 5. It follows that the PET image taken with MR $AC_{Dixon\text{-}GRAPPA}$ is useful for the attenuation correction of PET image. In addition, the reduction in PET average count mostly occurred from the bottom position due to the MR breast RF coil and PET/MR table. In this regard, Zhang *et al.* reported that the PET signal is decreased by the MR hardware and MR table [22]. In conclusion, our results confirmed that the MR $AC_{Dixon\text{-}GRAPPA}$ sequence results in effective PET images when using the MR breast RF coil during PET/MR scanning.

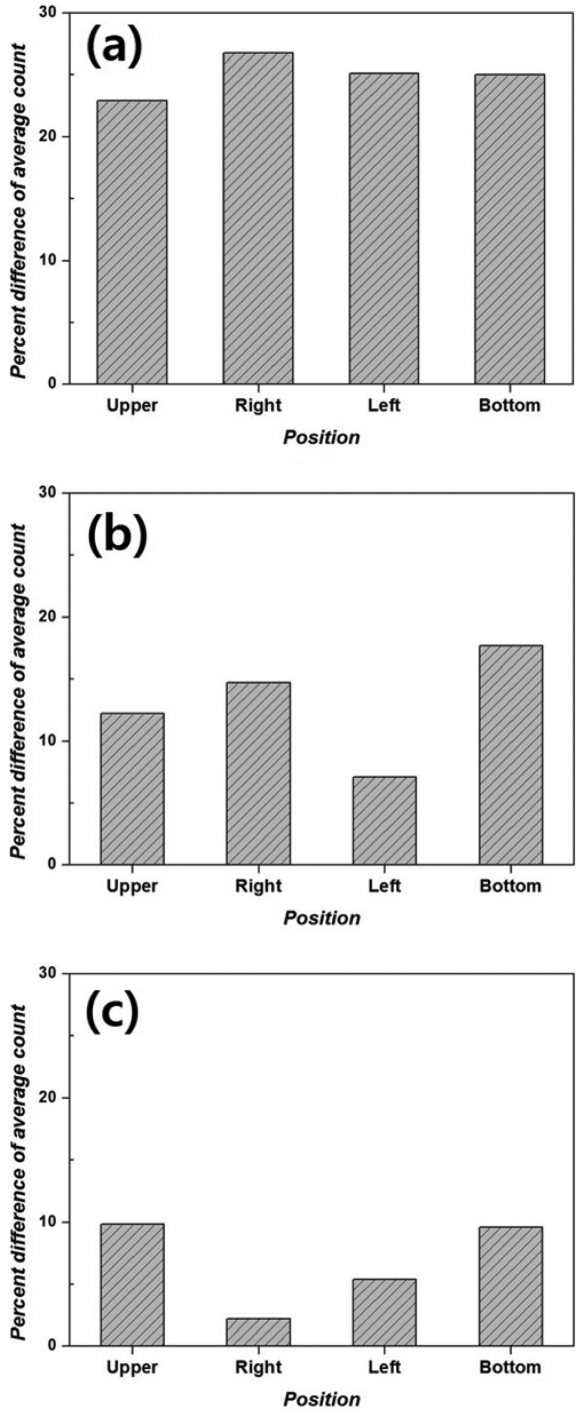

Fig. 7. Percentage difference in average count according to position with and without the MR breast RF coil, as follows: (a) MR $AC_{Dixon\text{-}CAIPI}$, (b) MR AC_{UTE}, and (c) MR $AC_{Dixon\text{-}GRAPPA}$.

Acknowledgment

The study was supported by the research foundation of Korea University.

References

[1] Y. Berker, J. Franke, A. Salomon, M. Palmowski, H. C. W. Donker, Y. Temur, F. M. Mottaghy, C. Kuhl, D. Izquierdo-Garcia, Z. A. Fayad, and F. Kiessling, J. Nucl. Med. **53**, 5 (2012).
[2] H. Zaidi and A. D. Guerra, Med. Phys. **38**, 10 (2011).
[3] R. Grazioso, N. Zhang, J. Corbeil, M. Schmand, R. Ladebeck, M. Vester, G. Schnur, W. Renz, and H. Fischer, Nuclear Instruments and Methods in Physics Research A **569**, 2 (2006).
[4] G. Antoch and A. Bockisch, Eur. J. Nucl. Med. Mol. Imaging **36**, 1 (2009).
[5] C. K. Kuhl, Radiology **244**, 2 (2007).
[6] C. K. Kuhl, Radiology **244**, 3 (2007).
[7] B. Aklan, D. H. Paulus, E. Wenkel, H. Braun, B. K. Navalpakkam, S. Ziegler, C. Geppert, E. E. Sigmund, A. Melsaether, and H. H. Quick, Med. Phys. **40**, 2 (2013).
[8] G. Delso, A. Martinez-Möller, R. A. Bundschuh, R. Ladebeck, Y. Candidus, D. Faul, and S. I. Ziegler, Phys. Med. Biol. **55**, 15 (2010).
[9] I. Dregely, T. Lanz, S. Metz, M. F. Mueller, M. Kuschan, M. Nimbalkar, R. A. Bundschuh, S. I. Ziegler, A. Haase, S. G. Nekolla, and M. Schwaiger, Eur. Radiol. **25**, 4 (2014).
[10] M. Oehmigen, M. E. Lindemann, T. Lanz, S. Kinner, and H. H. Quick, Med. Phys. **43**, 8 (2016).
[11] A. Ferguson, J. McConathy, Y. Su, D. Hewing, and R. Laforest, J. Nucl. Med. Technol. **42**, 8 (2014).
[12] J. P. J. Carney, D. W. Townsend, V. Rappoport, and B. Bendriem, Med. Phys. **33**, 4 (2006).
[13] B. D. Coombs, J. Szumowski, and W. Coshow, Mag. Reson. Med. **38**, 6 (1997).
[14] A. Martinez-Möller, M. Souvatzoglou, G. Delso, R. A. Bundschuh, C. Chefd'hotel, S. I. Ziegler, N. Navab, M. Schwaiger, and S. G. Nekolla, J. Nucl. Med. **50**, 4 (2009).
[15] M. A. Griswold, P. M. Jakob, R. M. Heidemann, M. Nittka, V. Jellus, J. Wang, B. Kiefer, and A. Haase, Mag. Reson. Med. **47**, 6 (2002).
[16] F. A. Breuer, M. Blaimer, M. F. Mueller, N. Seiberlich, R. M. Heidemann, M. A. Griswold, and P. M. Jakob, Mag. Reson. Med. **55**, 3 (2006).
[17] F. A. Breuer, M. Blaimer, R. M. Heidemann, M. F. Mueller, M. A. Griswold, and P. M. Jakob, Mag. Reson. Med. **53**, 3 (2005).
[18] D. J. Tyler, M. D. Robson, R. M. Henkelman, I. R. Young, and G. M. Bydder, J. Magn. Reson. Imaging **25**, 2 (2007).
[19] V. Keereman, Y. Fierens, T. Broux, Y. D. Deene, M. Lonneux, and S. Bandenberghe, J. Nucl. Med. **51**, 5 (2010).
[20] A. Waldman, J. H. Rees, C. S. Brock, M. D. Robson, P. D. Gatehouse, and G. M. Bydder, Neuroradiology **45**, 12 (2003).
[21] M. D. Robson and G. M. Bydder, NMR. Biomed. **19**, 7 (2006).
[22] B. Zhang, D. Pal, Z. Hu, N. Ojha, T. Guo, G. Muswick, C. Tung, and J. Kaste, IEEE Nuclear Science Symposium Conference Record (NSS/MIC) (2009).